Article

Reduced Graphene Oxide Decorated with Dispersed Gold Nanoparticles: Preparation, Characterization and Electrochemical Evaluation for Oxygen Reduction Reaction

Oana-Andreea Lazar [1], **Adriana Marinoiu** [2,*], **Mircea Raceanu** [2], **Aida Pantazi** [1],
Geanina Mihai [1], **Mihai Varlam** [2] **and Marius Enachescu** [1,3]

[1] Center for Surface Science and Nanotechnology, University Politehnica of Bucharest, 060042 Bucharest, Romania; oana.lazar@cssnt-upb.ro (O.-A.L.); aida.pantazi@cssnt-upb.ro (A.P.); geanina.mihai@cssnt-upb.ro (G.M.); marius.enachescu@cssnt-upb.ro (M.E.)
[2] RD Institute for Cryogenics and Isotopic Technologies-ICSI, 4 Uzinei St., 240050 Rm Valcea, Romania; mircea.raceanu@icsi.ro (M.R.); mihai.varlam@icsi.ro (M.V.)
[3] Academy of Romanian Scientists, 50085 Bucharest, Romania
* Correspondence: adriana.marinoiu@icsi.ro; Tel.: +40-774017659

check for updates

Abstract: The commonly used electrode Pt supported on a carbon (Pt/C) catalyst has demonstrated underperforming electrochemical durability in proton exchange membrane fuel cell (PEMFC) harsh operation conditions, especially in terms of Pt electrochemical instability and carbon corrosion. Gold nanoparticles (AuNPs) are considered one of the best alternative catalysts of PtNPs due to their remarkable selectivity for oxygen reduction reaction (ORR) and electrochemical stability in strong acid conditions, attributes which are ideal for practical PEMFC applications. In this work, we propose a new, facile and low-cost approach to prepare AuNPs supported on reduced graphene oxide nanocompounds (AuNPs/rGO). The morphological and structural properties of the as-prepared AuNPs/rGO were studied using various microscopic and spectroscopic techniques, namely, Raman Spectroscopy, Scanning Electron Microscopy (SEM), Scanning Transmission Electron Microscopy (STEM), X-Ray Diffraction (XRD), Fourier Transform Infrared Spectroscopy (FTIR), specific surface area (Brunauer–Emmett–Teller, BET). A mesoporous structure with narrow pore size distribution centered at 2 nm approximately, where the pores are regular and interconnected was successfully fabricated. The prepared catalyst was exposed to an accelerated stress test (potential cycles between −0.8 and +0.2 in KOH 1 M solution). The voltammetric stability test indicated a slight degradation after 1500 cycles. The electrochemical stability was assigned to the combined effect of AuNPs formed during chemical synthesis and to graphene oxide support.

Keywords: catalyst; fuel cell; graphene; gold nanoparticles

1. Introduction

The continuously growing worldwide interest for fuel cells utilized for power generation in a full range, of applications reflects the fact that these electrochemical devices are now on the threshold of the anticipated outcomes and therefore, ready for marketing. The emerging proton exchange membrane fuel cell (PEMFC) technology is more present in applied research, which is evidence that actual PEMFCs already hold the necessary reliability to compete with the existing engine and turbine technologies.

One of the dominant elements affecting the performance and durability of PEMFCs is the slow oxygen reduction reaction (ORR). Despite intensive research in the development of electrocatalytic

systems for ORR, particularly with respect to potential applications in PEMFC, there are still many important issues to be resolved [1–3]. Due to the fact that the commercial ORR catalysts still use Pt, the improvement of catalytic stability and activity should be addressed. Furthermore, the long-term durability has become the addressing key to the global sustainability of the FC systems.

A suitable metal as ORR electrocatalyst must not only provide both activity and selectivity, but, moreover, it should be stable into the severe environment in long-term PEMFC conditions (generated by oxidants, substantial acidic conditions appearing at inferior pH, accelerated potential variations, especially on the cathode, reactive radicals). Primarily, only several metals are able to avoid dissolving at the low pH and high electrode potentials which happens, especially at the cathode. In these conditions, poor stability is instantly understood as a loss in kinetic activity. The thermodynamic stability of various metals at different applied voltages and pH conditions were studied and described in Pourbaix diagrams. According to these diagrams, noble metals, namely, gold, iridium and platinum are very stable during the FC conditions (high potential, inferior pH), while metals, including Co, Ni, and Fe, are prone to dissolution [1]. It was experimentally demonstrated that the mentioned metals are electrochemically stable in the potential range of 0.3–1 V at low pH. Although, there are also other acid-stable metals, their poor catalytic activities or selectivity, demonstrated in PEMFC applications in comparison with Pt, are making them inappropriate in this regard.

On the other hand, it is known that only platinum elements, especially Au are stable enough in the ORR environment at the desirable operating potential of the cathode. Although Au fulfills the electrochemical stability requirement to develop a durable electrode, unfortunately, it is not very active toward ORR. Thus, the Au catalyst could be activated toward ORR by depositing it on reactive catalytic support. Not surprisingly, one of the most relevant aims of the Department of Energy is to increase the dissolution potential at the cathode. Taking into account this challenge, Au supported on the proper reactive surface could become more active and could contribute to developing much more stable ORR cathode. Up until now, the identifying of a particular ORR catalyst more electrochemically stable and active than the existing ones is still a complex challenge, since even with the *state-of-the-art* or presumed best ORR catalysts so far, between 30% and 40% of the energy released by the ORR reaction is wasted [4]. The dissolution of the catalyst is a temperature-dependent process, thus, catalysts with larger V_{diss} could predict higher durability in PEMFC.

However, what must be mentioned, based on the research regarding the thermodynamic stability, is that the Au noble metal has proven to be the most stable metal against dissolution because its dissolution potential, V_{diss}, (1.5 V vs. SHE) is much higher than the U_{diss} for Pt (1.18 V vs. SHE). Therefore, despite a supposedly poor catalytic activity of Au versus Pt in PEMFC, we aim to fabricate an ORR electrocatalytic system based on Gold nanoparticles (AuNPs) deposited on good catalytic support with improved performances and to evaluate it in respect to electrochemical stability.

The actual effectiveness and long-term performance of catalytic sites are dependent on the selected support [5–7]. In order to obtain good catalytic activity and carbon corrosion resistance, the equilibrium between the graphitic level, the number of surface oxide species, pore size, surface roughness and hydrophobicity have to be taken into consideration [8–12]. The cathode catalyst layer has the primary impact on this equilibrium.

The reduced graphene oxide (rGO) has obtained much scientific consideration in the last years as a support material, mainly due to its suitable properties in respect to durability issues in PEMFC, such as already oxidized stage and stable characteristics in strongly-acidic media [13–17]. The high porosity of the oxidized form of graphene is recommended for potential application as support for metal nanoparticles, therefore it is adequate support for small Au nanoparticles anchoring, used for further ORR evaluation. Studies dealing with the preparation of small AuNPs in mild conditions are limited, and those presenting excellent ORR activity are even more limited [18–20]. The explanation could be related to the difficulty in synthesizing uniform small-size AuNPs. A few attempts to incorporate AuNPs into the carbon holes of rGO layers alongside the investigation of their ORR performances were

presented in the literature so far. However, the agglomeration of AuNPs and graphene restacking, which cause a low utilization of AuNPs still are the main unresolved problems.

Therefore, Au deposited on reduced graphene oxide (AuNP/rGO) appears as a special electrochemically stable nanomaterial for PEMFC for two reasons: (i) The ORR catalytic activity is highly based on active sites of the revealed area and on the large area to volume ratio, thus the small dimensions of Au particles provide a spectacular advantage; (ii) using a surface capping agent as binder or stabilizer, AuNPs/rGO could have improved resistance to agglomeration and dissolution, thus leading to reliable stability, which is advantageous for durable cycling of the potential during the ORR electrochemical process.

In the present study, we developed a simple and low-cost approach to prepare AuNPs/rGO nanocomposites through the in situ reduction of graphene oxide and chloroauric acid using a compatible cationic polyelectrolyte, namely, poly-diallyldimethylammonium chloride as a conductive polymer binder.

The successful preparation of the AuNPs/GO nanocomposite was confirmed by different studies carried out through various microscopic and spectroscopic techniques, namely, Scanning Electron Microscopy (SEM), Scanning Transmission Electron Microscopy (STEM), X-Ray Diffraction (XRD), Raman Spectroscopy and Fourier Transform Infrared Spectroscopy (FTIR). The other objective was a preliminary assessment to evaluate the potential of further developing of ORR electrodes for PEMFC. The stability of potential fuel cell catalysts is still an important target, thus, the prepared catalyst was exposed to an accelerated stress test consisting of 1500 potential cycles between −0.8 and +0.2 in 1 M KOH. The cyclic voltammograms during stability test indicated a minor degradation after 1500 cycles.

2. Materials and Methods

2.1. Catalyst Synthesis

The fabrication of gold nanoparticles supported on reduced graphene oxide nanocomposites (AuNPs/rGO) is presented. The detailed description of the first intermediary compound, graphite oxide, was presented in our previous research [21–25]. The Graphite oxide material was prepared from natural graphite using the modified Hummers method. In this respect, graphite flakes (KOH–I-NOR Grafit S.R.O) were mixed with 300 mL H_2SO_4 (Sigma-Aldrich, St. Louis, MO, USA, min.98%), 32 g $K_2S_2O_8$ (Sigma-Aldrich, St. Louis, MO, USA, 99%), 35 g P_2O_5 (Fluka, 98%), under vigorous stirring. The mixture was heated at 80 °C, and then cooled. 30 g $KMnO_4$ (Sigma-Aldrich, St. Louis, MO, USA, ACS, 99.0% min) has been added gradually keeping the temperature up to 10 °C, and then the reaction mass was heated to 50 °C. The H_2O_2 (30% aqueous solution, Sigma-Aldrich, St. Louis, MO, USA) was introduced, and the color of the solution became dark yellow. The solid was separated and washed several times. The dispersion containing graphite oxide was exfoliated to multi-layered graphene oxide (GO), by ultra-sonication (110 W/40 kHz, 30–40 °C). AuNPs/rGO nanocomposites were prepared by in situ reduction of GO and chloroauric acid ($HauCl_4 \cdot xH_2O$, Alfa Aesar, 99.9%) using a compatible cationic polyelectrolyte, namely, poly-diallyldimethylammonium chloride (Sigma-Aldrich, St. Louis, MO, USA 20wt.% in water) used as well as a binder. The poly-diallyldimethylammonium chloride (PDDA) solution (170 mL) was introduced in the reaction mass, which was then ultrasonically mixed for 60 min. The chloroauric acid was introduced to the dispersed mixture (under continuing stirring). Sodium borohydride ($NaBH_4$ 98 wt.%, Fluka) was added as a reducing agent. The reduction reaction was performed at 80 °C for 4 h, and then the reaction mass was cooled and separated by ultracentrifugation (16,000 rpm). AuNPs/rGO sample was obtained as the final product.

2.2. Physical-Chemical Characterization

A Hitachi SU 8230 Field Emission Scanning Electron Microscope was used to perform the morphological and compositional characterization of the sample. For the SEM micrographs, two detectors were used: A secondary electron one–SE(U) and a backscattered electron one–HA(T) at

an accelerating voltage of 10 kV. Also, a Hitachi HD-2700 Scanning Transmission Electron Microscope (STEM) with cold field emission electron gun was used for the acquired images at an accelerating voltage of 200 kV and 10 μA emission current. The STEM images were recorded by using three different detectors: Secondary electrons (SE), phase contrast (ZC) and transmission electrons (TE) at the same location on the sample at the same magnification on the studied sample. The structural investigation was carried out on prepared samples and SEM, Z Contrast and TEM images were obtained. For the X-Ray Diffraction measurements, the samples were analyzed using a Rigaku SmartLab X-Ray Diffractometer with a copper target (λ = 0.1540598 nm), a tube voltage of 45 kV, a tube current of 200 mA, and a K_β filter. The diffractograms were fitted using SmartLab Studio Software from Rigaku and compared with existing data from the PDF2 database and literature. The ATR-FTIR spectra of the samples were recorded at room temperature using a Perkin–Elmer Spectrum Two IR spectrometer. Attenuated total internal reflection FTIR measurements were performed by averaging 25 scans, with a resolution of 4 cm^{-1}, over the 4000–450 cm^{-1} wavenumber range. The thermogravimetric analysis (TGA) was done using a Perkin Elmer STA 8000 in the air with a rate of 5 °C/min in the range 50–900 °C. The analysis was realized using 5 mg of AuNPs/rGO composite in an alumina crucible. The micro-Raman studies of GO and Au doped GO samples were performed at ambient temperature by using a LabRam HR800 system with a high-resolution confocal micro-Raman Spectroscopy. The Raman spectra were produced by exposing the specimens during 100 s to a 0.8 mW, 632 nm wavelength red excitation laser and dispersing the sample emitted signal onto the CCD detector using a 600 lines/mm grating. The quantitative determination of Au from the AuNPs/rGO nanocomposite was performed using the flame atomic absorption spectroscopy (Varian AA 240 FS DUO spectrometer). The sample (50 mg) was mineralized in the microwave digestion system (Millestone 1200 MEGA), in the presence of a mixture of acids: sulfuric acid, perchloric acid and hydrogen fluoride. The power program chosen was: 5 min /250 W–5 min /400 W–10 min/500 W. The standard addition method was used. A gold standard with a concentration of 1000 ppm was taken into consideration. For an accurate and sure C, H, N, S and O determination, Thermo Scientific FLASH 2000 organic elemental analyzer with argon, as a carrier gas, was used. The surface area measurement has been done using the Autosorb IQ (Quantachrome) through the BET technique. The nitrogen adsorption-desorption isotherms are provided. The samples were degassed prior to analysis (115 °C and 4 h). The specific surface area was calculated using the Brunauer–Emmett–Teller (BET) equation, using the linearity criterion in the P/P_ range of 0.1–0.3, while the Barrett-Joyner-Halenda (BJH) equation and functional theory of density (DFT) were involved in completing the studies of textural properties. The pore size distribution was investigated by taking into account the equations corresponding to the theory of the BJH method and the quenched solid density functional theory (QSDFT) assuming cylindrical, slit and combined-shape models for the pores of the graphene-based materials.

2.3. Electrochemical Characterization

The electrocatalytic behavior of AuNP/rGO was investigated by cyclic voltammetry (CV) method using a conventional three-electrode electrochemical cell. The cyclic voltammetry (CV) was carried out using a potentiostat/galvanostat (VersaScan electrochemical workstation). In this three-electrode system, Pt wire, Ag/AgCl electrode and AuNp/rGO were used as a counter, reference and working electrodes, respectively. 10 μL of AuNP/rGO suspension (5 mg AuNP/rGO, 250 μL propanol, 26 μL 5% Nafion solution, 2 mL demineralized water) was dropped onto the pre-polished electrode (geometric area: 0.0707 cm^2). All electrochemical experiments were carried out in 1 M KOH electrolyte.

3. Results and Discussion

In order to characterize the nanostructure of the prepared sample and to determine the presence of the metal, the Scanning Transmission Electron Microscopy (STEM) technique was used. The results that are presented in Figure 1 give information about the structured properties (topographical and morphological properties) of the AuNPs/rGO sample. These images were recorded at the same position

on the sample at ×15 K and ×3000 K magnifications using secondary electrons detector–SE (on the left), phase contrast detector–ZC (in the middle) and transmission detector–TE (on the right).
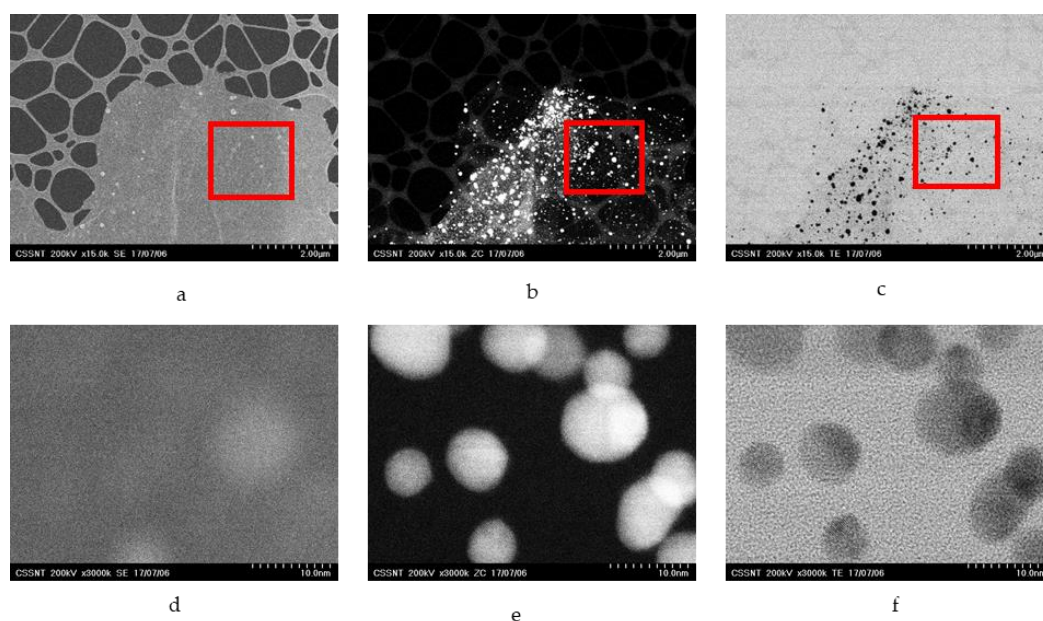
Figure 1. STEM electron micrographs of the reduced graphene oxide nanocompounds (AuNPs/rGO) at the same location at different magnifications: Secondary electrons (SE)—(**a**,**d**), phase contrast (ZC)—(**b**,**e**), and transmission electrons (TE)—(**c**,**f**).

Figure 2 represents the distribution of Au nanoparticles diameter sizes. The size distribution of Au NPs was extracted from STEM images by measuring around 500 individual nanoparticles. The spherical geometry of Au NPs was also determined from STEM investigations.
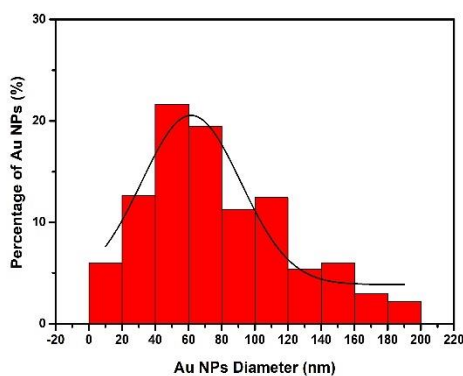
Figure 2. Distribution of the AuNPs percentage by their diameter sizes.

The Au NPs diameter sizes, determined based on STEM analysis, were found to be ranged from 4 nm to 200 nm.

The chart was best fitted with a Gauss function, exhibiting a unimodal distribution of AuNPs. The highest percentage of NPs were found to be within 41–60 nm and 61–80 nm diameter size ranges, as it can be seen in Figure 2, having the mean diameter sizes of 51.4 ± 4.5 nm and 71.7 ± 5.4 nm, respectively.

Table 1 provides the mean AuNPs diameter sizes corresponding to each diameters range and their standard deviation.

Table 1. Statistical quantities extracted from the Au NPs size distribution: The range of diameters, percentage of Au NPs, mean diameter size, and standard deviation of mean diameter size.

Diameters Range (nm)	Percentage of Au NPs (%)	Mean Diameter Size (nm)	Standard Deviation (nm)
0–20	6.01	12.3	±5.5
21–40	12.62	31.5	±7
41–60	21.64	51.4	±4.5
61–80	19.44	71.7	±5.4
81–100	11.22	89.3	±4.6
101–120	12.42	110.7	±5.1
121–140	5.41	128.9	±4.1
141–160	6.01	147.1	±4.3
161–180	3	170.5	±8.8
181–200	2.2	189.1	±8.4

In Figure 3a,c the ultra-high-resolution STEM images, obtained on Gold nanoparticles supported on graphene oxide, using transmission electron microscopy technique at ×6000 k and ×7000 k magnifications, are presented. These electron images which were recorded in the areas marked with red in Figure 1a–c, show a good spatial distribution of Au nanoparticles on the graphene flakes.
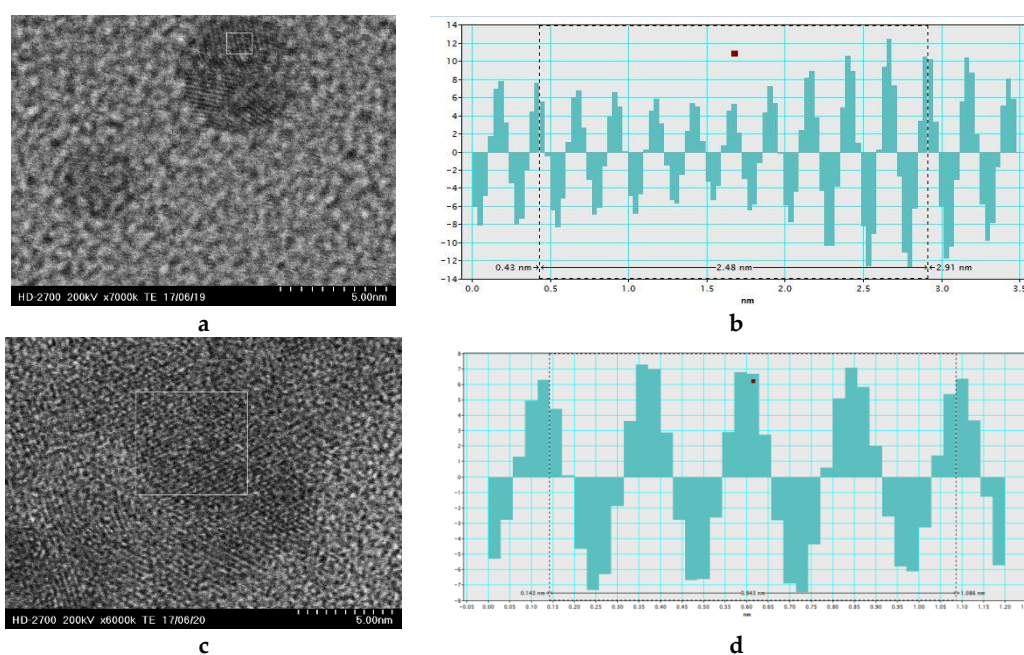
Figure 3. (**a,c**) Ultra-High-Resolution (UHR)–STEM electron micrographs of the AuNPs/rGO (**b,d**) Interplanar-distance profiles for Au and graphene, respectively.

In the first profile (b), from Figure 3, the value of 2.48 Å d-spacing characteristic for the plane (111) of Au nanoparticles with face-centered cubic structure was determined. In the second profile (d) the value of 2.35 Å d-spacing characteristic for single layer reduced graphene oxide was measured. Also, the high-resolution STEM images which are shown in Figure 3a,c give information about the interplanar distance of the prepared sample. The interplanar distance marked in the first profile corresponds to the plane (111) face-centered cubic structure of gold nanoparticles, which is in good agreement with the XRD results shown below, in Figure 4 [23].
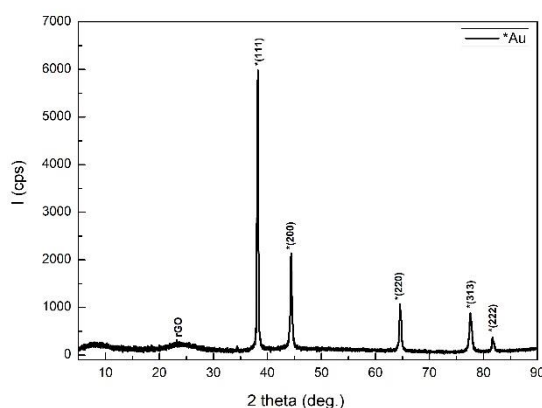
Figure 4. XRD Diffractograms of AuNPs/rGO.

In the XRD diffractogram the peak for rGO is present at 2θ = 23.54° corresponding to the (002) orientation [26]. The presence of Au is shown by the diffraction peaks at 38.18°, 44.39°, 64.58°, 77.55° and 81.72°, corresponding to the (111), (200), (220), (313) and (222) orientations, respectively, identified using PDF No 00-004-0784 [27].

For the study of the presence of functional groups at the basal plane of the rGO after the reduction process, Fourier Transform Infrared spectroscopy (FTIR) measurements were acquired on both rGO and AuNPs/rGO, and the spectra are shown in Figure 5. The peaks present in both spectra at 2345 cm^{-1}, 1960 cm^{-1}, 1725 cm^{-1} and 1573 cm^{-1}, correspond to C=C=C, C=C=O or C≡C vibration, C=C vibration, C=O carbonyl stretching and C=C stretching, respectively. Between the rGO and the AuNPs/rGO there is a peak shift from 1144 cm^{-1} (C-H wag) to 1062 cm^{-1} (C-N stretch). Also, the transmittance is higher in the AuNPs/rGO sample. The absence of the 3450 cm^{-1} peak shows the fact that the GO was reduced, this peak is an indicator of the O–H stretch [26,28–30].
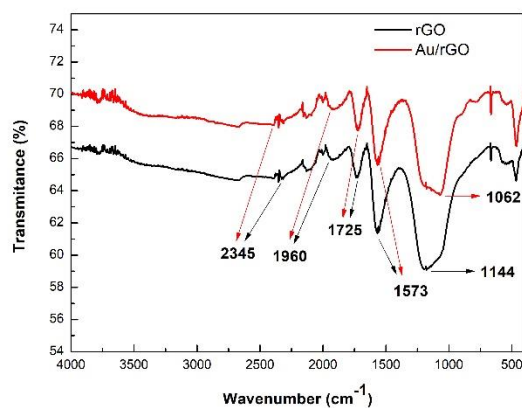
Figure 5. FTIR Spectra of rGO (in black) and of AuNPs/rGO (in red).

The morphological study of the AuNPs/rGO sample was also done by the SEM, and the results are presented in Figure 6. The micrographs were achieved with two detectors: SE (a, c, e, g-left) which give information about the morphology of the sample and HA-BSE—high angle-backscattered electron (b, d, f, h-right) which has an emphasis on compositional information, at the same location on the sample at 3k×, 5k×, 20k× and 100k× magnifications.
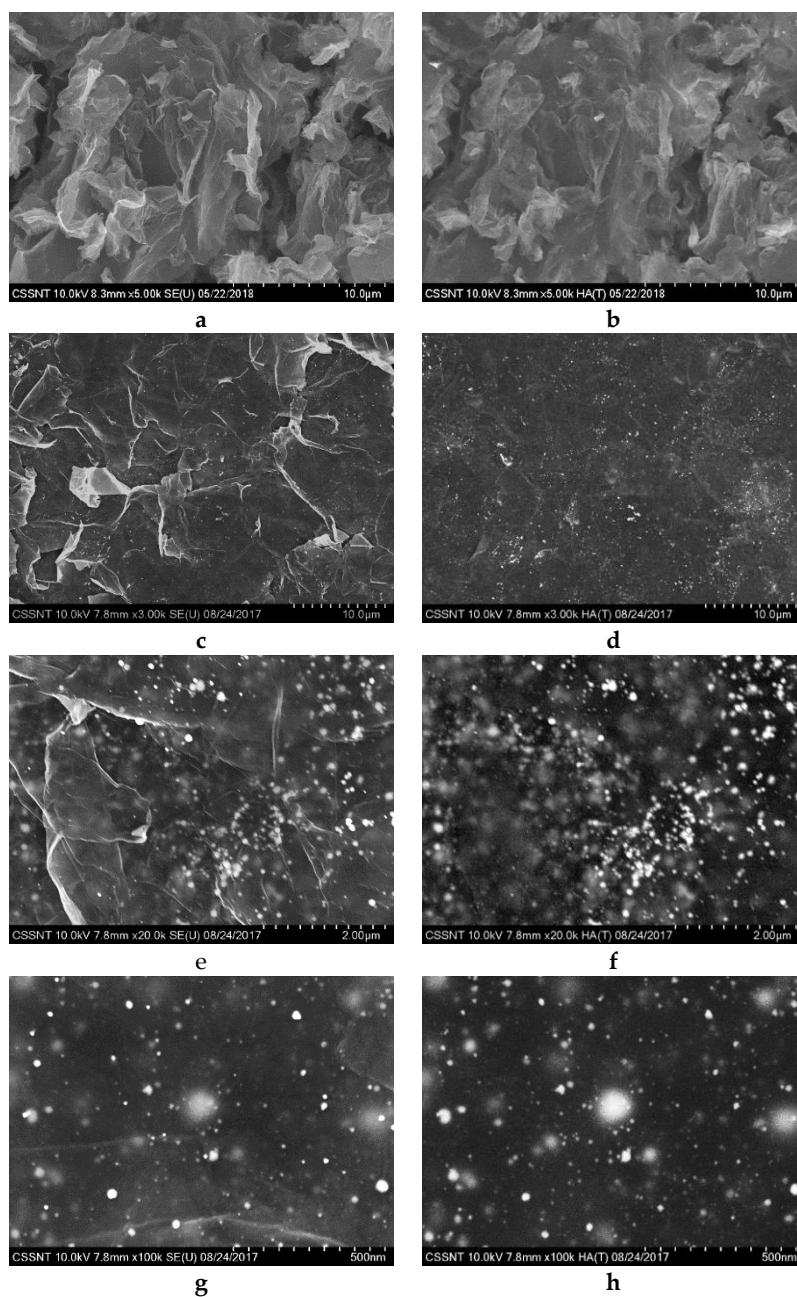
Figure 6. SEM micrographs of rGO (**a**,**b**) and AuNP/rGO (**c–h**): Left–SE–morphology information, right–HA-BSE–compositional information.

SEM micrographs of the AuNPs/rGO show the ultrathin GO sheets with the presence of Au nanoparticles with a size range from 5 to 100 nm. In the SEM micrographs, the graphene sheets are clearly visible. The rGO sheets seem to be arranged in a random porous architecture, their morphology being composed of a range of folds and wrinkles. This morphology shows an excellent connected network of flakes which is important for the PEMFC application, namely, for the necessary electronic transport.

Also, the porous architecture entices a homogenous distribution of the AuNPs, which can be seen especially well in the micrographs obtained using the HA-BSE detector (Figure 6c–h–right). These micrographs of the AuNPs/GO show an ultrathin GO sheet with the presence of Au nanoparticles of sizes in the range 5–100 nm.

The thermogravimetric analysis (TGA) graphs (Figure 7) show mass profiles of powder samples as a modification of temperature. As described in the literature [26,29], the slow weight loss, ~10%,

observed in the interval 50–400 °C is caused, most likely, by the small amount of oxygen functional groups in the rGO's structure. A sharp decrease in weight, ~50%, appears between 400° and 560 °C. As the derivate has only one peak, we can conclude that there is only one material that burns, namely, the rGO at 560 °C. The remnant mass is 41.71%, and it could represent the amount of Au, as the maximum heating temperature of the analysis (900 °C) is smaller than the melting point of gold, 1064 °C.
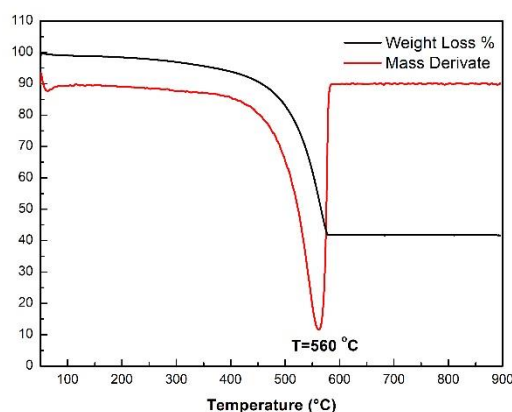
Figure 7. TGA Curve of AuNPs/rGO.

The quantitative determination of gold was supplementary performed by flame atomic absorption spectroscopy. The data demonstrated the presence of similar content. The elemental composition of prepared AuNPs/rGO was analyzed by elemental analysis (C, O, H, N) and the results are listed in Table 2.

Table 2. Chemical composition for AuNPs/rGO.

Sample	Elemental Composition (wt.%)					
	Elemental Analysis			TGA Analysis		Atomic Absorption Spectroscopy
AuNP/rGO	C	O	H	N	Au	Au
	38.83	12.82	3.95	2.69	41.71	40.23

The Raman spectra, shown in Figure 8, exhibits the Raman signature of graphitic materials [31,32] labeled by three principle bands attributed to the first order D and G modes, and the second-order 2D mode. The G mode has E_{2g} symmetry and arises as a result of the in-plane stretching vibration of carbon atoms bonds. This band is common for all sp^2 carbon systems. The D band (A_{1g} symmetry) represents the in-plane breathing mode of the aromatic six carbon atom rings (sp^3). This band becomes active only in the presence of any disorder from a perfect structure. Therefore, it could be considered a defect or disorder-induced band. The intensity of the D band is growing relative to the G band, with the increasing degree of disorder in the graphitic structure. The 2D mode is the second order of the D band, but unlike D band, the 2D band is not activated by the proximity to a defect.

The micro-Raman spectra of both samples, rGO and AuNPs/rGO, show an intense and broad D band, reflecting the density of defects within materials' structure which, most likely, are induced by the presence of oxygen-containing functional groups [33] and Graphene-Au nanoparticles interactions [34], respectively. The positions, widths and intensities of the peaks were precisely identified from the spectra deconvolutions (see Figures 9 and 10) obtained using the Peak Fit software, after performing a linear baseline correction.
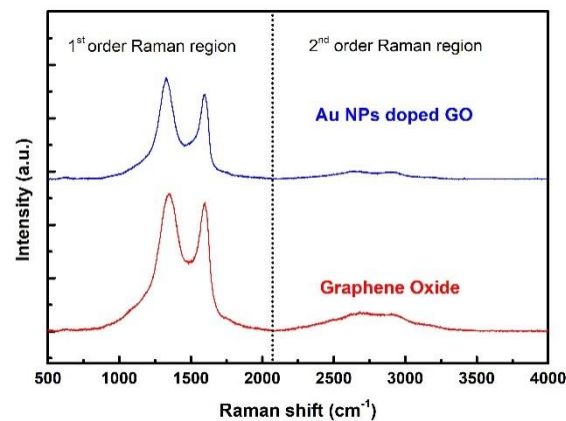
Figure 8. Micro-Raman spectra of graphene oxide and Au nanoparticles doped rGO samples.
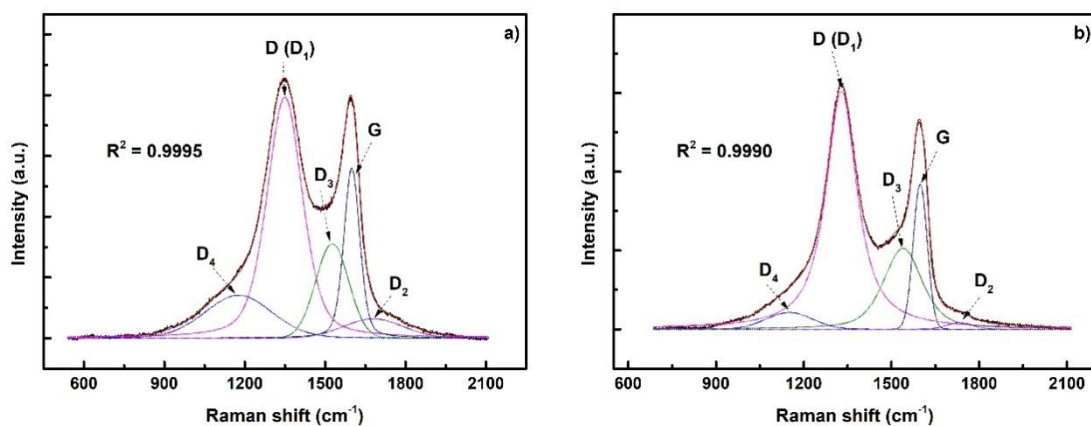
Figure 9. Deconvolution of the first-order Raman region for: (**a**) GO and (**b**) AuNPs/rGO samples. Sum of the deconvolution is marked with the red line.
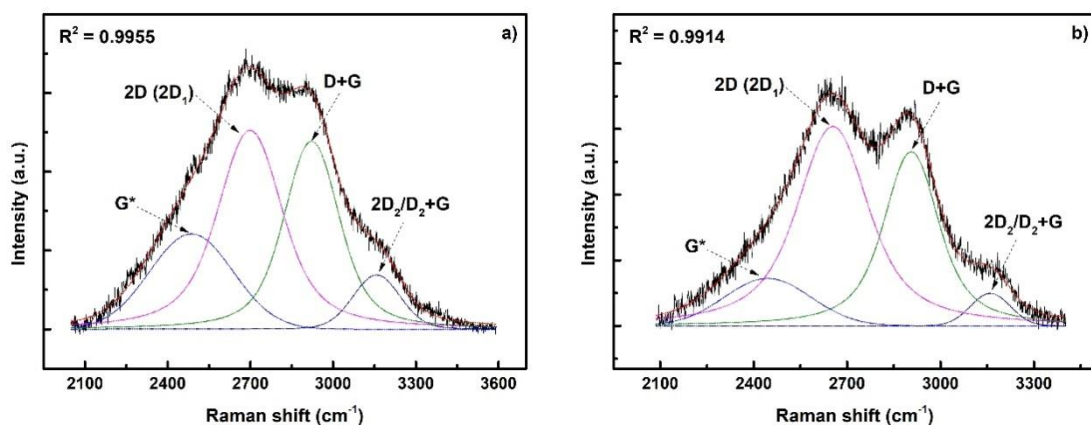
Figure 10. Deconvolution of the second-order Raman region for: (**a**) GO and (**b**) AuNPs/rGO samples. Sum of the deconvolution is marked with the red line.

The first order Raman region (up to 2000 cm^{-1}) was deconvoluted to five peaks (see Table 3) using a combined Gauss and Lorentz function. The peaks centered at 1349/1329 and 1599/1598 cm^{-1} are attributed to the conventional D (D$_1$ band) and G modes. The G band shows a shoulder at ~1680/1733 cm^{-1}, which is typical for defective graphitic structures. The component, called D$_2$ band, is clearly proven in the deconvolution of the Raman spectra of both samples, rGO and AuNPs/rGO, as presented in Figure 9. The D$_2$ band was assigned to the lattice vibrations of the graphene layers which

are not interleaved between two other graphene layers [35]. For a complete analysis of the materials, two additional bands located at~1176/1150 cm^{-1} and~1526/1539 cm^{-1} revealed by the deconvolution of the first spectral region, were considered. According to the work reported by Dippel et al. [36], these bands, so-called D_3 and D_4, respectively could be associated to the C-C and C=C stretching vibration modes. On the other hand, D_3 band could be attributed to the presence of the disordered amorphous carbon in the studied materials [37]. All the observed D bands are activated by different disorder effects, such as edge vibrations, defects in or between the hexagonal planes, heteroatoms, etc.

Table 3. Position of the first order Raman bands and their full widths at half maximum.

Sample	Peak Position/FWHM (cm^{-1})				
	D_4	D (D_1)	D_3	G	D_2
GO	1176/294	1349/156	1526/144	1599/69	1680/262
AuNP/rGO	1150/186	1329/127	1539/156	1598/57	1733/104

The second order Raman region (from 2000 up to 3500 cm^{-1}) was best fitted to four peaks (see Table 4) using a Voigt function. The first two signals at 2485/2444 cm^{-1} and 2698/2654 cm^{-1} are assigned to G* and 2D Raman modes [38], respectively. In a single layer of graphene, the 2D band appears as a single symmetric band, but in this case, due to the sample shape (multi-layered graphene stacks), this band splits into several modes. The splitting of this band is caused by the symmetry lowering, which occurs with the increase of the number of graphene layers. The band at 2922/2906 cm^{-1} was assigned to D + G mode [39]. The peak at 3160 cm^{-1} has been assigned to the G + D_2 mode.

Table 4. Position of the second order Raman bands and their full widths at half maximum.

Sample	Peak Position/FWHM (cm^{-1})			
	G*	2D ($2D_1$)	D + G	G + D_2
GO	2485/356	2698/278	2922/237	3157/201
AuNP/rGO	2444/327	2654/273	2906/209	3160/150

"G*" is a notation for the second order Raman mode shown in Figure 10, and it is different from the conventional G mode for the carbon based materials.

The level of disorder in the studied materials was quantified using the intensity ratios of D and G bands [40], as presented in Table 4. The I_{D_1}/I_G intensity ratio calculated for Au doped GO sample (1.64) is higher than the one obtained for the as-prepared GO (1.41). This increase in the defect density could be attributed to the successfully anchoring of Au nanoparticles.

The intensity ratio of D_1 and D_2 bands describes the nature of the defects present in the structure of the materials. The I_{D_1}/I_{D_2} intensity ratio for GO sample was found to be approximately 13. This value is indicating the presence of sp^3 defects [41]. The Au NPs decorated GO sample reveals a significantly higher I_{D_1}/I_{D_2} intensity ratio (~36), which suggests a higher level of disorder in graphene's structure. This difference could also confirm the successful incorporation of Au nanoparticles.

The in-plane sp^2 crystallite size, L_a, was calculated for both investigated materials (see Table 4), using the following formula, which is suitable for disordered carbon materials [42]:

$$L_a = 2.4 \times 10^{-10} \times \lambda_L^4 \times \left(\frac{I_D}{I_G}\right)^{-1},$$

where λ_L is the excitation wavelength.

Both, G and D bands have a sharper profile (see Table 3) for the doped sample when compared to pristine GO. This increase in frequency together with the FWHM decrease for the G band as a result of the doping process can be explained by the energy enhancement of the phonons that contribute to the peak, due to the non-adiabatic character of the photon perturbation which in turn removes the

Kohn anomaly. This happens due to the shifts in Fermi level away from the Dirac point introduced by the doping process and reduces the recombination probability of the excited charge carriers [43]. The decrease in crystallite size (see Table 5) calculated for the doped sample compared to the pristine GO can be correlated with the G and D bands sharpening.

Table 5. The I_{D_1}/I_G intensity ratios, the crystallite sizes, La, and the I_{D_1}/I_{D_2} intensity ratios.

Material	I_{D_1}/I_G Ratio	Crystallite Size, L_a (nm)	I_{D_1}/I_{D_2} Ratio
GO	1.41	27	13
AuNP/rGO	1.64	23	36

A slight decrease in intensity of G and D bands could be observed in the Raman spectra recorded for the sample decorated with Au nanoparticles. This decrease could be correlated with the presence of the metal nanoparticles into the graphene structure, as it is known that Au cannot be detected using the Raman spectroscopy.

Taking into account the porous appearing of the prepared AuNPs/rGO settled by the previous measurements, the specific surface area has been afterwards considered. Usually, catalytic systems with a high surface area can be obtained either by fabrication of small particles where each particle has a high surface-to-volume ratio, or by producing materials where the void surface area (pores) are high relative to most of the support material volume. Gas adsorption analysis using nitrogen was employed to determine the surface area and porosity. The absorption isotherm with both adsorption–desorption branches is provided in Figure 11. The big hysteresis between curves clearly indicates the existence of mesoporosity (pores in the range 2–50 nm). The sharp rise at low values P/P_0 indicates a high surface area, while the abrupt loading transition within P/P_0 range of 0.4–0.5 reveals a unimodal pore size distribution.
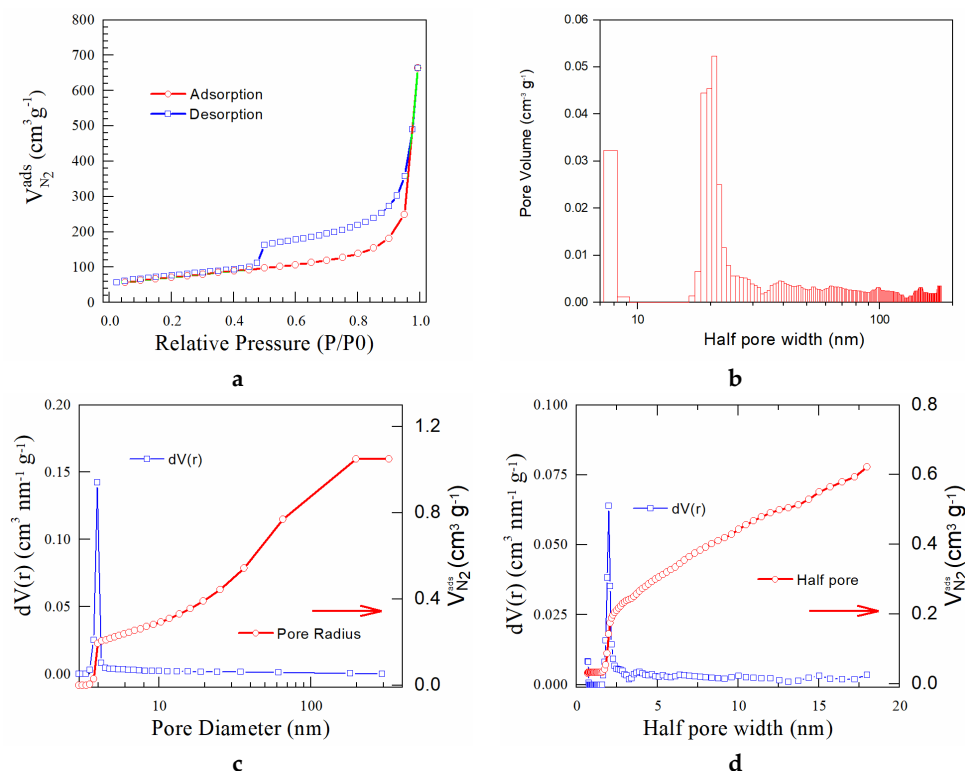
Figure 11. Nitrogen adsorption and desorption isotherms (**a**) and the pore size distributions for AuNPs/rGO (**b**–**d**). (**a**) Nitrogen adsorption-desorption isotherms BET (Brunauer–Emmett–Teller). (**b**) Histogram for pore-size distribution obtained using the QSDFT model. (**c**) Pore size distribution (BJH method). (**d**) Pore size distribution (QSDFT method).

A lesser extent for micropores in the prepared material was noticed, deriving from the vertical uptake under $P/P_0 = 0.04$. In addition, Barret-Joyner-Halenda (BJH) method was carried out to analyze the porous composition of AuNPs/rGO (Table 6). The evaluation indicated mainly a mesoporous structure, while the pores are regular with narrow pore size distribution centered at 2 nm approximately. The pores in the Au-functionalized graphene were interconnected (which is in good agreement with SEM results) and extended from the inside to the surface of the materials. This porous structure is expected to be helpful for electrochemical reactions, especially for ORR. The observations suggest good transport properties among the primary and secondary pores with complementary roles in ORR transport properties.

Table 6. Textural properties of AuNPs/rGO.

S_{BET} [a] $(m^2 g^{-1})$	Pore Size Distribution Data Estimated by Using BJH Method		Pore Size Distribution Data Estimated by Using DFT Method	
	Pore Volume [b] $(cm^3 g^{-1})$	Pore Radius Dv(r) [b] (nm)	Pore Volume [c] $(cm^3 g^{-1})$	Pore RadiusDv(r) [c] (nm)
246	1.049	1.857	0.621	1.9845

[a] Calculated considering the linear part of the BET plot ($P/P_0 = 0.1$–0.3). [b] Calculated by applying the BJH method (employing of the N_2 volume adsorbed at $P/P_0 = 0.99$). [c] Calculated by applying the DFT method (employing the N_2 volume adsorbed at $P/P_0 = 0.99$).

The pores structure characterization was supplementary evaluated using the capabilities of the advanced quenched solid density functional theory method, which takes into consideration the roughness and heterogeneity of the nanocarbons pore wall surfaces. The estimated pore size distribution with BJH and DFT (presented in Figure 11) indicated that the calculated average pore width (presented in Table 6) are very close (1.857 nm and 1.984 nm, calculated using BJH and DFT, respectively) and moreover, their magnitude was located within microporous materials. However, the pore volumes differ somewhat (1.049 $cm^3 g^{-1}$ and 0.621 $cm^3 g^{-1}$, calculated using BJH and DFT, respectively), which demonstrate the necessity of applicability of both models for a comprehensive textural evaluation.

The electrochemical stability of catalysts under practical operating conditions is one of the key factors for commercialization and extensive use of FCs. The prepared AuNPs/rGO obtained according to the experimental part, were subjected to a preliminary electrochemical characterization for the evaluation of electrocatalytic active area (ECSA). It is expected that anchoring the Au nanoparticles on graphene oxide will affect the electrochemically accessible area (ECSA), thus it is necessary to investigate how they relate with the support area. The electrocatalytic activity of AuNP/rGO was investigated by using cyclic voltammetry (CV) scanning in 1 M KOH aqueous solution with different potential values in the range from −0.8 mV to 0.2 mV (E/V vs. Ag/AgCl) in order to analyze the interfacial properties. During the CV experiment, the scan rate was changed, and very good responses were obtained. Figure 12 presents the CV curves acquired at different values of scan rate (25, 50, 75, 100 mV/s). Oxidative peak potentials and reductive peak potentials were well separated and very sensitive to the scan rate.

The large reduction peaks observed at approximately −0.45 V could be attributed mainly to the reduction of the oxygen functional groups of graphene oxide, which increased gradually with scan rate. This was explained by the deposition of AuNPs with high conductivity on GO support [20].

Characteristic reduction peaks at approx. −0.2 V (vs. Ag / AgCl) with onset potential at approx. −0.09 V were easily observed, indicating the electrocatalytic activity of the prepared catalyst for ORR. By using the scan rates in the range from 25 mV/s to 100 mV/s, an increase of the peak current and of the negative shift of peak potential was obtained. The formation of the second reduction peak at lower potentials (~0.2 V vs. Ag/AgCl) is caused by the ORR process. The linear relationship between the peak current I_p and scan rate suggests that the diffusion-controlled process at the electrode surface is

the predominant reaction (inserted plot in Figure 11). The reduction peaks observed at approximately -0.2 V could be assigned to the reduction process of Au^{+3}, leading to the formation of AuNPs on the electrode surface.
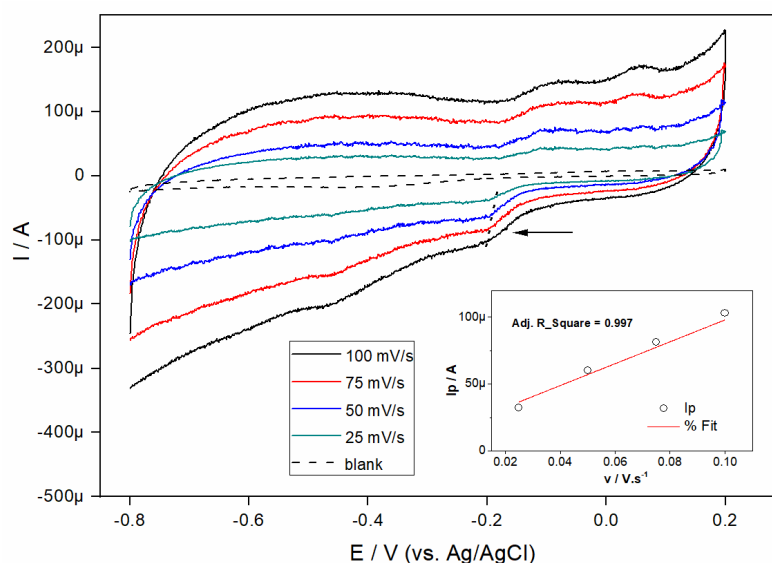
Figure 12. Cyclic voltametric response of AuNP/rGO sample at different scan rate.

ECSA value is the main information of the utilization of precious metals with minimal metal loading. Thus, this result indicates a better utilization of active Au-sites in Au/rGO catalyst most likely due to the high specific surface area according to BET analysis and to better dispersion of Au NPs according to TEM analysis. $ECSA_{AuNP/rGO}$ was estimated in Table 7 (i) taking into account the load for the single layer of hydrogen adsorption as 390 μC cm^{-2} [44], and (ii) considering the linear dependence between the highest current and the scan velocity.

Table 7. Cyclic voltammetry studies for Au/rGO at different values of scan rates.

Scan Velocity (mV/s)	E Initial (mV)	E Final (mV)	I_P (µA)	Surface (µC)	Electrode Surface Calculation	
					Q/q (cm^2)	ECSA (m^2/g)
25	-0.533	-0.219	-46	295	0.756	19.3
50	-0.581	-0.226	-85	293	0.751	18.15
75	-0.590	-0.224	-101	274	0.702	17.9
100	-0.595	-0.216	-121	261	0.699	17.83
-	-	-	-	-	Average	18.3

The electrochemical surface area of AuNP/rGO electrode was calculated using the charge associated with the reduction of gold oxide by integration, which is proportional to the real active surface area of the gold surface.

The obtained results in the mass transport region could be attributed to the synergistic effect of nano-sized Au as co-catalyst and 3D porous structure of rGO support. Adding the AuNPs as co-catalyst could lead to significant charge carrier concentration in π-band of rGO layers, based on the metallic nature, which means the obtaining of better electrical contacts.

The impedance test was carried out in the frequency range of 0.1 Hz to 100 kHz at open-circuit potential, as presented in Figure 13. The Nyquist plots were performed for blank electrode, rGO and AuNP/rGO; the obtained curves indicate a depressed semicircle for rGO and AuNP/rGO in the region of high frequency and a vertical line in the region of low frequency. The smaller semicircle in the

case of AuNP/rGO suggests excellent electrical conductivity and a lower resistance value of the composite material.
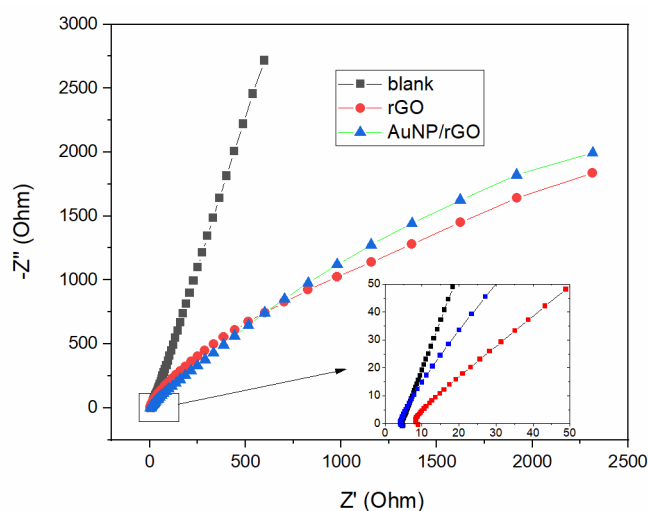
Figure 13. EIS results for bare electrode, rGO and AuNP/rGO in a solution of KOH 1M.

It is necessary to be mentioned that the reduced graphene oxide support can serve as electroactive sites, and it also reduces the ion diffusion pathway, also resulting in quick conduction.

The stability of potential FC catalysts is an important target, thus, the prepared catalyst Au/rGO was exposed to an accelerated stress test, which consisted of 1500 potential cycles between −0.8 and +0.2 in 1 M KOH. The results are presented in the Figure 14. The signals corresponding to Au reactions (hydrogen and oxygen reactions) slightly decreased with time of stability indicating a minor degradation after 1500 cycles.

Gold supported on graphene oxide materials demonstrates a significant contribution to the basic scientific research of electrochemical stability of graphene-based materials with relevance in developing of the ORR electrode. Future research will be targeted to explore gold modified electrodes as regards the effect of gold loading, and application of the graphene-based materials in ORR reactions.
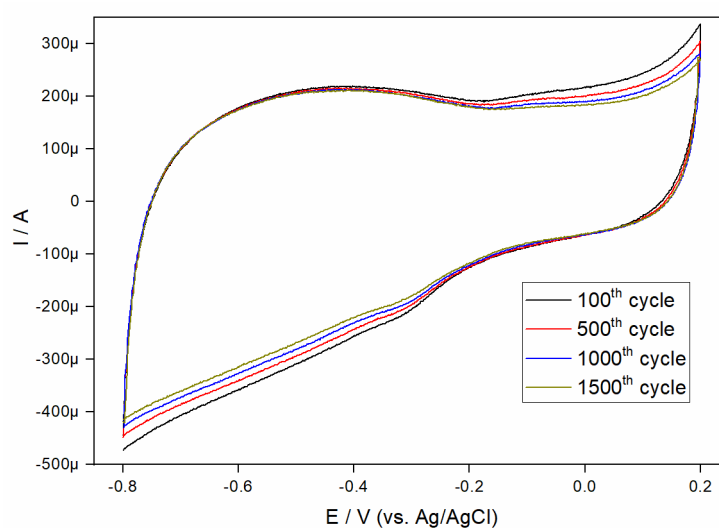
Figure 14. Voltammetric stability test of AuNP/rGO; conditions: 1 M KOH solution, 200 mV s^{-1}.

4. Conclusions

AuNPs/rGO nanocompounds were prepared by a new and simple approach. STEM and SEM images indicated an excellent distribution of AuNPs on the layered graphene oxide sheets. The successful anchoring of the Au nanoparticles into graphene sheets was also confirmed by the Raman studies. The AuNPs/rGO with high specific surface area, with a mesoporous structure with narrow pore size distribution centered at 2 nm approximately where the pores are regular and interconnected were successfully fabricated. The experimental results on voltammetric stability indicated a slight degradation after accelerated stress test consisting in 1500 potential cycles between -0.8 and $+0.2$ in KOH 1 M solution. The prepared catalyst could be considered one of the best alternative catalysts of PtNPs, due to their remarkable ex-situ electrochemical stability after 1500 cycles, attributes which are ideal for developing electrodes for PEMFC applications.

Author Contributions: Conceptualization, A.M.; methodology, software, M.R.; validation, M.V.; investigation, A.P., O.-A.L., G.M. and A.M.; writing—original draft preparation, A.M.; writing—review and editing, A.P., O.-A.L., G.M. and M.E.; supervision, M.E. All authors have read and agreed to the published version of the manuscript.

Conflicts of Interest: The authors declare no conflict of interest.

References

1. Holton, O.T.; Stevenson, J.W. The role of platinum in proton exchange membrane fuel cells. *Platin. Met. Rev.* **2013**, *57*, 259–271. [CrossRef]

2. Wang, Y.-J.; Zhao, N.; Fang, B.; Li, H.; Bi, X.T.; Wang, H. Carbon-Supported Pt-Based Alloy Electrocatalysts for the Oxygen Reduction Reaction in Polymer Electrolyte Membrane Fuel Cells: Particle Size, Shape, and Composition Manipulation and Their Impact to Activity. *Chem. Rev.* **2015**, *115*, 3433–3467. [CrossRef]

3. Tang, Z.; Wu, W.; Wang, K. Oxygen Reduction Reaction Catalyzed by Noble Metal Clusters. *Catalysts* **2018**, *8*, 65. [CrossRef]

4. Campbel, T.; Alcantara Ortigoza, M.; Stolbov, S. Au/Ta (110) and Au/Nb (110) as Highly Active, Stable, and Inexpensive Catalysts for Oxygen Reduction Reaction on Hydrogen Fuel Cell Cathodes: Prediction from First Principles. *ChemCatChem* **2020**, *12*, 1743–1749. [CrossRef]

5. Rao, C.N.R.; Sood, A.K.; Subrahmanyam, K.S.; Govindaraj, A. Graphene: The New Two-Dimensional Nanomaterial. *Angew. Chem. Int. Ed.* **2009**, *48*, 7752–7777. [CrossRef] [PubMed]

6. Ghosh, A.; Basu, S.; Verma, A. Graphene and Functionalized Graphene Supported Platinum Catalyst for PEMFC. *Fuel Cells* **2013**, *13*, 355–363. [CrossRef]

7. Marinoiu, A.; Raceanu, M.; Teodorescu, C.; Ebrasu, D.; Varlam, M.; Stefanescu, I. *Graphene-Supported Platinum Catalysts for Fuel Cells Applications*; CNR: Bologna, Italy, 2015.

8. Zhang, Y.; Chen, S.; Wang, Y.; Ding, W.; Wu, R.; Li, L.; Qi, X.; Wei, Z. Study of the degradation mechanisms of carbon-supported platinum fuel cells catalyst via different accelerated stress test. *J. Power Sources* **2015**, *273*, 62–69. [CrossRef]

9. Shao, Y.; Wang, J.; Kou, R.; Engelhard, M.; Liu, J.; Wang, Y.; Lin, Y. The corrosion of PEM fuel cell catalyst supports and its implications for developing durable catalysts. *Electrochim. Acta* **2009**, *54*, 3109–3114. [CrossRef]

10. Dai, L. Functionalization of Graphene for Efficient Energy Conversion and Storage. *Acc. Chem. Res.* **2013**, *46*, 31–42. [CrossRef]

11. Takabatake, Y.; Noda, Z.; Lyth, S.M.; Hayashi, A.; Sasaki, K. Cycle durability of metal oxide supports for PEFC electrocatalysts. *Int. J. Hydrogen Energy* **2014**, *39*, 5074–5082. [CrossRef]

12. Zhao, X.; Hayashi, A.; Noda, Z.; Kimijima, K.; Yagi, I.; Sasaki, K. Evaluation of change in nanostructure through the heat treatment of carbon materials and their durability for the start/stop operation of polymer electrolyte fuel cells. *Electrochim. Acta* **2013**, *97*, 33–41. [CrossRef]

13. Marinoiu, A.; Raceanu, M.; Carcadea, E.; Varlam, M.; Soare, A.; Stefanescu, I. Doped graphene as non-metallic catalyst for fuel cells. *Medziagotyra* **2017**, *23*, 108–113. [CrossRef]

14. Schonvogel, D.; Hülstede, J.; Wagner, P.; Dyck, A.; Agert, C.; Wark, M. Durability of Electrocatalysts for ORR: Pt on Nanocomposite of Reduced Graphene Oxide with FTO versus Pt/C. *J. Electrochem. Soc.* **2018**, *165*, F3373. [CrossRef]

15. Marinoiu, A.; Cobzaru, C.; Carcadea, E.; Raceanu, M.; Atkinson, I.; Varlam, M.; Stefanescu, I. An experimental approach for finding low cost alternative support material in PEM fuel cells. *Rev. Roum. Chim.* **2015**, *61*, 433–440.

16. Marinoiu, A.; Gatto, I.; Raceanu, M.; Varlam, M.; Moise, C.; Pantazi, A.; Jianu, C.; Stefanescu, I.; Enachescu, M. Low cost iodine intercalated graphene for fuel cells electrodes. *Appl. Surf. Sci.* **2017**, *424*, 93–100. [CrossRef]

17. Marinoiu, A.; Gatto, I.; Raceanu, M.; Varlam, M.; Moise, C.; Pantazi, A.; Jianu, C.; Stefanescu, I.; Enachescu, M. Low cost iodine doped graphene for fuel cell electrodes. *Int. J. Hydrogen Energy* **2017**, *42*, 26877–26888. [CrossRef]

18. Kim, S.-S.; Kim, Y.-R.; Chung, T.D.; Sohn, B.-H. Tunable Decoration of Reduced Graphene Oxide with Au Nanoparticles for the Oxygen Reduction Reaction. *Adv. Funct. Mater.* **2014**, *24*, 2764–2771. [CrossRef]

19. Fujigaya, T.; Kim, C.; Hamasaki, Y.; Nakashima, N. Growth and Deposition of Au Nanoclusters on Polymer-wrapped Graphene and Their Oxygen Reduction Activity. *Sci. Rep.* **2016**, *6*, 2–11. [CrossRef]

20. Lee, C.S.; Yu, S.H.; Kim, T.H. One step Electrochemical Fabrication of Reduced Graphene Oxide/Gold Nanoparticles Nanocomposite-Modified Electrode for Simultaneous Detection of Dopamine, Ascorbic and Uric Acid. *Nanomaterials* **2018**, *8*, 17. [CrossRef]

21. Marinoiu, A.; Raceanu, M.; Carcadea, E.; Varlam, M.; Balan, D.; Ebrasu, D.; Stefanescu, I.; Enachescu, M. Iodine Doped Graphene for Enhanced Electrocatalytic Oxygen Reduction Reaction in PEM Fuel Cell Applications. *J. Electrochem. Energy Convers Storage* **2017**, *14*, 031001. [CrossRef]

22. Marinoiu, A.; Raceanu, M.; Carcadea, E.; Marinescu, D.; Teodorescu, C.; Mellichio, A.; Varlam, M.; Stefanescu, I. Convenient graphene based materials as potential candidates for low cost fuel cell catalysts. *React. Kinet. Mech. Catal.* **2016**, *118*, 281–296. [CrossRef]

23. Marinoiu, A.; Raceanu, M.; Carcadea, E.; Pantazi, A.; Mesterca, R.; Tutunaru, O.; Ion, S.; Bala, D.; Varlam, M.; Enachescu, M. *Noble Metal Dispersed Reduced Graphene Oxide and Its Application in PEM Fuel Cells*; InTechOpen: London, UK, 2018; ISBN 978-953-51-6257-5.

24. Marinoiu, A.; Raceanu, M.; Carcadea, E.; Varlam, M. Iodine-doped grapheme—Catalyst layer in PEM fuel cells. *Appl. Surf. Sci.* **2018**, *456*, 238–245. [CrossRef]

25. Borup, R.; Meyers, J.; Pivovar, B.; Kim, Y.S.; Mukundan, R.; Garland, N.; Myers, D.; Wilson, M.; Garzon, F.; Wood, D.; et al. Scientific Aspects of Polymer Electrolyte Fuel Cell Durability and Degradation. *Chem. Rev.* **2007**, *107*, 3904–3951. [CrossRef] [PubMed]

26. Loryuenyong, V.; Totepvimarn, K.; Eimburanapravat, P.; Boonchompoo, W.; Buasri, A. Preparation and Characterization of Reduced Graphene Oxide Sheets via Water-Based Exfoliation and Reduction Methods. *Adv. Mater. Sci. Eng.* **2013**, *2013*, 923403. [CrossRef]

27. ICDD. *PDF2/Inorganic, Mineral, Alloy&Metal, Common Phase (Database)*; Kabekkodu, S., Ed.; International Centre for Diffraction Data: Newtown Square, PA, USA, 2014.

28. Muda, M.R.; Ramli, M.M.; Isa, S.S.M.; Jamlos, M.F.; Murad, S.A.Z.; Norhanisah, Z.; Isa, M.M.; Kasjoo, S.R.; Ahmad, N.; Nor, N.I.M.; et al. Fundamental study of reduction graphene oxide by sodium borohydride for gas sensor application. *AIP Conf. Proc.* **2017**, *1808*, 020034. [CrossRef]

29. Hu, N.; Yang, Z.; Wang, Y.; Zhang, L.; Wang, Y.; Huang, X.; Wei, H.; Wei, L.; Zhang, Y. Ultrafast and sensitive room temperature NH3 gas sensors based on chemically reduced graphene oxide. *Nanotechnology* **2014**, *25*, 025502. [CrossRef]

30. Yang, F.; Zhao, M.; Zheng, B.; Xiao, D.; Wu, L.; Guo, Y. Influence of pH on the fluorescence properties of graphene quantum dots using ozonation pre-oxide hydrothermal synthesis. *J. Mater. Chem.* **2012**, *22*, 25471–25479. [CrossRef]

31. Sun, Y.P.; Fu, K.; Lin, Y.; Huang, W. Functionalized Carbon Nanotubes: Properties and Applications. *Acc. Chem. Res.* **2002**, *35*, 1096–1104. [CrossRef]

32. Cioffi, C.; Campidelli, S.; Sooambar, C.; Marcaccio, M.; Marcolongo, G.; Meneghetti, M.; Paolucci, D.; Paolucci, F.; Ehli, C.; Rahman, G.A.; et al. Synthesis, Characterization, and Photoinduced Electron Transfer in Functionalized Single Wall Carbon Nanohorns. *J. Am. Chem. Soc.* **2007**, *129*, 3938. [CrossRef]

33. Ambrosi, A.; Bonanni, A.; Sofer, Z.; Cross, J.S.; Pumera, M. Electrochemistry at Chemically Modified Graphenes. *Chem. Eur. J.* **2011**, *17*, 10763–10770. [CrossRef]

34. Gutés, A.; Hsia, B.; Sussman, A.; Mickelson, W.; Zettl, A.; Carraro, C.; Maboudian, R. Graphene decoration with metal nanoparticles: Towards easy integration for sensing applications. *Nanoscale* **2012**, *4*, 438–440. [CrossRef] [PubMed]

35. Sadezky, A.; Muckenhuber, H.; Grothe, H.; Niessner, R.; Pöschl, U. Raman microspectroscopy of soot and related carbonaceous materials: Spectral analysis and structural information. *Carbon* **2005**, *43*, 1731–1742. [CrossRef]

36. Dippel, B.; Jander, H.; Heintzenberg, J.J. NIR FT Raman spectroscopic study of flame soot. *Phys. Chem. Chem. Phys.* **1999**, *1*, 4707. [CrossRef]

37. Jawhari, T.; Roid, A.; Casado, J. Raman spectroscopic characterization of some commercially available carbon black materials. *Carbon* **1995**, *33*, 1561. [CrossRef]

38. Malard, L.M.; Pimenta, M.A.; Dresselhaus, G.; Dresselhaus, M.S. Dresselhaus, Raman spectroscopy in graphene. *Phys. Rep.* **2009**, *473*, 51–87. [CrossRef]

39. Ferreira, E.H.M.; Moutinho, M.V.O.; Stavale, F.; Lucchese, M.M.; Capaz, R.B.; Achete, C.A.; Jorio, A. Evolution of the Raman spectra from single-, few-, and many-layer graphene with increasing disorder. *Phys. Rev. B* **2010**, *82*, 125429. [CrossRef]

40. Tuinstra, F.; Koenig, J.L. Raman Spectrum of Graphite. *J. Chem. Phys.* **1970**, *53*, 1126. [CrossRef]

41. Trusovas, R.; Račiukaitis, G.; Niaura, G.; Barkauskas, J.; Valušis, G.; Pauliukaite, R. Recent Advances in Laser Utilization in the Chemical Modification of Graphene Oxide and Its Applications. *Adv. Opt. Mater.* **2016**, *4*, 37–65. [CrossRef]

42. Giovanni, M.; Poh, H.L.; Ambrosi, A.; Zhao, G.; Sofer, Z.; Sanek, F.; Khezri, B.; Webster, R.D.; Pumer, M. Noble metal (Pd, Ru, Rh, Pt, Au, Ag) doped graphene hybrids for electrocatalysis. *Nanoscale* **2012**, *4*, 5002. [CrossRef]

43. Childres, I.; Jauregui, L.A.; Park, W.; Cao, H.; Chena, Y.P. *Raman Spectroscopy of Graphene and Related Materials*; Jang, J.I., Ed.; New Developments in Photon and Materials Research; Nova Science Publishers: Hauppauge, NY, USA, 2013.

44. Łukaszewski, M.; Soszko, M.; Czerwiński, A. Electrochemical Methods of Real Surface Area Determination of Noble Metal Electrodes—An Overview. *Int. J. Electrochem. Sci.* **2016**, *11*, 4442–4469. [CrossRef]